

ADAPTIVE CONTROLLER DESIGN FOR TRAJECTORY TRACKING IN A FUEL-CELL POWERED AUTOMOBILE

Srinivas Palanki¹ Panini K. Kolavennu,
David Cartes, John C. Telotte

*Department of Chemical and Biomedical Engineering,
FAMU-FSU College of Engineering, Florida State
University, Tallahassee, FL 32310-6046, USA*

Abstract: In this paper, a model reference adaptive controller is designed using the Lyapunov method, for tracking a time varying power profile in an automobile powered by a fuel cell. The adaptability of the controller is tested by implementing the controller on different power profiles which simulate actual power requirement of different road conditions. *Copyright ©2007 IFAC*

Keywords: adaptive control, PEM fuel cell, power generation system

1. INTRODUCTION

Fuel cell power systems for automotive applications have received increased attention in recent years because of their potential for high fuel efficiency and lower emissions [Zalc and Loffler, 2002]. While there have been significant advances in fuel cell technology, one reason this technology has not seen wide-spread applications in the automotive industry has been the lack of an efficient hydrogen distribution center and the difficulties associated with storing hydrogen onboard an automobile [Lovins and Williams, 1999]. One option to alleviate these problems is to develop a system that utilizes a commonly available carbon-based hydrogenous fuel such as gasoline or methane to generate the necessary hydrogen *in situ* on an “as needed” basis. In a previous paper [Kolavennu *et al.*, 2006a] we considered the design of a fuel-cell powered automobile that utilizes methane as a source of hydrogen. In this paper, an adaptive controller is developed that tracks the power trajectory of realistic road profiles in a fuel-cell powered automobile. In particular, it is shown

that the controller is able to track a variety of different road profiles without having to be tuned off-line.

2. SYSTEM DESIGN CONSIDERATIONS

A schematic of the fuel cell system under consideration is shown in Fig. 1. The two main components of the overall system are (1) the fuel processing subsystem and (2) the power generation subsystem. Methane enters the fuel processing subsystem and is converted to hydrogen. Hydrogen enters the fuel cell where it mixes with oxygen to generate electrical power which drives an electric motor. In addition to the fuel cell, there is a battery backup that the electric motor switches to when the hydrogen delivered to the fuel cell is insufficient to meet the *instantaneous* power demands of the electric motor. This battery backup is essential because significant load transitions occur frequently as a result of sudden acceleration on highway ramps as well as terrain changes [Zalc and Loffler, 2002]. The design of the battery backup is not addressed in this paper.

¹ Corresponding author: palanki@eng.fsu.edu

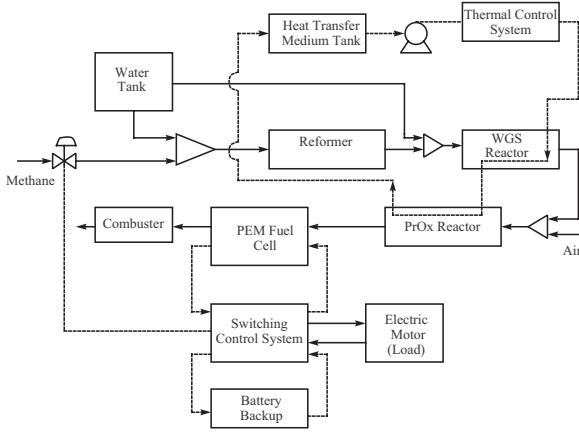


Fig. 1. Schematic of Fuel Cell System

In an earlier paper [Kolavennu *et al.*, 2006a], the primary components of a fuel cell power system, that utilizes methane to generate hydrogen, were analyzed. In particular, basic chemical engineering principles were utilized to design a reactor train that converts methane to hydrogen of the desired purity. The relation between power produced by a PEM fuel cell and methane entering the reactor train *at steady state* was calculated. However, a typical automobile does not operate at steady state. The power demand for an automobile motor undergoes significant variations due to acceleration, changes in road surface and traffic conditions.

In this paper, we analyze the power generation subsystem in the face of fluctuating power demand. When power demand goes down, the excess hydrogen can be diverted from the fuel cell. A sudden *increase* in power demand requires an instantaneous increase in hydrogen flow rate into the fuel cell. However, the conversion of methane to hydrogen takes several seconds which leads to an unacceptable lag between power demand of the motor and the power supplied by the fuel cell. For this reason, a backup battery is required that takes over this power load during the time it takes for the fuel cell to generate the necessary power. In a previous paper [Kolavennu *et al.*, 2006b] a logic-based switching controller was designed that switches to the battery backup when the fuel cell is unable to provide the necessary power to the motor. In this paper, we design a controller that adjusts the hydrogen flow into the fuel cell in response to changing power demand. This design is tested via simulations for several typical power profiles of an automobile motor.

Pukrushpan (2003) developed a dynamic model for a PEM fuel cell stack system similar to the one shown in Fig. 1. The transient phenomena captured in the model includes the flow characteristics and inertia dynamics of the compressor and the reactant partial pressures. Characterization of the fuel cell polarization curves based on

time varying current, partial oxygen and hydrogen pressures, temperature and membrane hydration allows for analysis of the transient fuel cell power generation.

The model developed by Pukrushpan (2003) consists of 78 differential and algebraic equations. After suitable substitution of variables, we obtained a reduced model of the fuel cell system that is a set of nine ordinary differential equations and is suitable for controller design and analysis. This model is shown in Appendix A. In this model, it is assumed that all the cells in the stack perform similarly, i.e., by analyzing the polarization curve of a single cell, the stack performance can be estimated. The power from the fuel cell, which is a function of the current and voltage, is given by:

$$P = V_{st}I = (N_c V_c)(iA_c) \quad (1)$$

where P is the power produced by the fuel cell, V_{st} is the voltage of the stack which is the product of the number of cells N_c and the individual cell voltage V_c , I is the current drawn from the cell and is the same for each cell and depends on the area of cross section A_c , i is the current density.

The reversible standard potential E^o for the above cell reaction is 1.23 V at 25 °C as determined from the change in the Gibb's free energy. The actual voltage depends upon the concentration of the species and temperature at which the fuel cell is operating. The concentration dependence is given by the Nernst equation (Pukrushpan, 2003) as shown below:

$$E = 1.229 - 8.5 \times 10^{-4}(T_{fc} - 298.15) + 4.3085 \times 10^{-5}T_{fc} \left[\ln(P_{H_2}) - \frac{1}{2}\ln(P_{O_2}) \right] \quad (2)$$

where E is the open circuit voltage, the fuel cell temperature T_{fc} is in K, and reactant partial pressures P_{H_2} and P_{O_2} are expressed in atm. The actual cell voltage at any given current density is obtained by subtracting the activation, ohmic and concentration losses from the reversible potential as expressed below.

$$v_{fc} = E - v_{act} - v_{ohm} - v_{conc} \quad (3)$$

where v_{act} , v_{ohm} and v_{conc} are activation, ohmic and concentration overvoltages. These losses are a function of the current density, pressure, membrane humidity and also on the type of membrane and are represented by the empirical equations given below

$$v_{act} = v_0 + v_a(1 - e^{-10i}) \quad (4)$$

$$v_{ohm} = i.R_{ohm} \quad (5)$$

$$v_{conc} = i \left(c_2 \frac{i}{i_{max}} \right)^2 \quad (6)$$

where v_0 , v_a and c_2 are functions of temperature, pressure and membrane humidity of the cell. Us-

ing this model we can calculate the power produced by the fuel cell based on the voltage current characteristics. For a given current demand the voltage is calculated using Eq. 3 and thereby the power output of the fuel cell.

3. CONTROLLER DESIGN FOR POWER GENERATION SUBSYSTEM

For the fuel cell systems to operate at levels comparable to existing internal combustion engines, the key issue that should be addressed is the *transient* behavior of fuel cell systems. Automobiles are subjected to significant load transitions during operation and the fuel cell system should be able to produce power which can follow this varying load profile. Power produced by the fuel cell is dependent on the voltage current characteristics. The transient response data from the nonlinear model presented in Appendix A was generated by subjecting the nonlinear system to a series of step inputs in the current around the 100 Amperes operating point. Utilizing this input output data from the nonlinear model system identification techniques were employed to derive a linear second order model was fit between the current demand and the voltage produced by the fuel cell stack. The transfer function G_p is given below

$$G_p = \frac{-390.78}{s^2 + 27.291s + 2068.8} \quad (7)$$

This transfer function is used in this paper to design an adaptive controller to regulate the power output of the fuel cell to the power demand. This adaptive controller is then implemented on the *nonlinear* model described in Appendix A. The control problem is to track the power demand of the motor using current as the manipulated variable.

To get a more realistic power vs time profile we obtained the power profile for a small car from an existing speed vs time profile using ADVISOR software package [NREL, 2002] as shown in Figure 2. The Urban Dynamometer Driving schedule(UDDS) which is designed for light duty vehicle testing in city driving conditions was used.

Model reference adaptive control (MRAC) is derived from the model reference control (MRC) problem. The objective of MRC is to find the feedback control law that changes the structure and dynamics of the plant so that its I/O properties are exactly the same as those of a reference model. The structure of an MRC scheme for a LTI, SISO plant is shown in Fig. 3 [Ioannou and Sun, 1996]. Here, $W_m(s)$ is the transfer function of the reference model, $r(t)$ a given reference input signal, $y_m(t)$ the output of the reference model

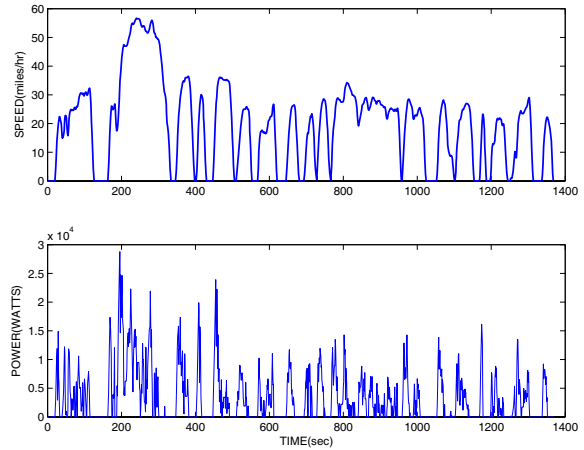


Fig. 2. Speed and Power Profile for UDDS

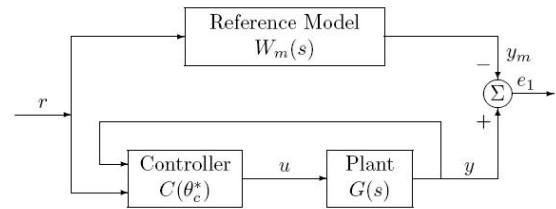


Fig. 3. Model Reference Adaptive Control

and $y(t)$ is the plant output. The feedback controller, denoted by $C(\Theta_c)$, is designed so that all signals are bounded and the closed-loop plant transfer function from r to y is equal to $W_m(s)$. This transfer function matching guarantees that for any given reference input $r(t)$, the tracking error $e = y - y_m$, which represents the deviation of the plant output from the desired trajectory y_m , converges to zero with time.

Simulations with the nonlinear model shown in Appendix A indicated that the system had a time constant of 0.023 s. Thus, the model reference is chosen to be:

$$W_m = \frac{1}{s + 0.023} \quad (8)$$

The performance of the adaptive controller can be improved by adding some derivative action, i.e., using a PD controller in conjunction with the adaptive controller. This essentially makes the linearized plant represented by eq. 7 of unity relative degree which is the same as that of the reference model eq. 8.

The following analysis for the stability and adaptation law for the combined PD and adaptive controllers is along the lines of Ioannou and Sun (1996). Consider the plant equation given by a second order transfer function

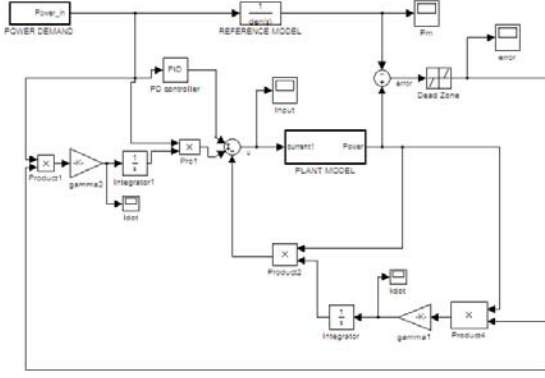


Fig. 4. Adaptive Controller with Derivative Action

$$y_p = G_p(s)u_p \quad \text{where} \quad (9)$$

$$G_p(s) = \frac{b}{s^2 + a_1s + a_2} \quad (10)$$

If a PD controller is added to adaptive action as shown in Fig. 4, the new control input to the system is given by

$$u_p = \bar{k}y_p + \bar{l}r + k_c(y_p - r) + K_d s(y_p - r) \quad (11)$$

Without loss in generality, this can be written as

$$u_p = k^*y_p + l^*r + k_d s y_p - k_d s r \quad (12)$$

Substituting this value of u_p into Eq. 9, we can calculate the closed loop transfer function between y_p and r as

$$(s^2 + a_1s + a_2)y_p = b(k^*y_p + l^*r + k_d s y_p - k_d s r) \quad (13)$$

This implies

$$y_p = \frac{b(l^* - s k_d)}{s^2 + (a_1 - k_d b)s + (a_2 - b k^*)} r \quad (14)$$

The control objective is to track the reference model output

$$y_m = \frac{b_m}{s + a_m} r \quad (15)$$

Equating the right hand sides of Eq. 15 and Eq. 14 we get

$$\frac{b(l^* - s k_d)}{s^2 + (a_1 - k_d b)s + (a_2 - b k^*)} r = \frac{b_m}{s + a_m} r \quad (16)$$

which implies

$$\begin{aligned} (-k_d b)s^2 + b(l^* - a_m k_d)s + a_m l^* b = \\ b_m s^2 + b_m(a_1 - k_d b)s + a_2 - b k^* \end{aligned} \quad (17)$$

Equating the coefficients of s^n on both sides we have the optimal values for k_d , l^* , k^*

$$k_d = \frac{-b_m}{b} \quad (18)$$

$$l^* = \frac{b_m}{b}(a_1 + b_m - a_m) \quad (19)$$

$$k^* = \frac{a_2 - a_m l^* b}{b} \quad (20)$$

The optimal values of k_d , l^* , k^* when substituted in Eq. 13 ensure that the plant output follows the model output. Hence if k^* and l^* are exactly known then $y_p = y_m$ and we have

$$(s^2 + a_1s + a_2)y_m = b(k^*y_p + l^*r + k_d s y_p - k_d s r) \quad (21)$$

In reality, k^* and l^* are not known. If k and l are estimates of k^* and l^* , then

$$(s^2 + a_1s + a_2)y_p = b(ky_p + lr + k_d s y_p - k_d s r) \quad (22)$$

Subtracting Eq. 21 from Eq. 22 and replacing $y_p - y_m$ with e , we have

$$(s^2 + a_1s + a_2)e = b(\tilde{k}y_p + \tilde{l}r) \quad (23)$$

where

$$\tilde{k} = k - k^*; \quad \tilde{l} = l - l^*; \quad (24)$$

This can be expressed in state space form as

$$\dot{X} = A_c X + B_c \tilde{\theta}^T \omega \quad (25)$$

$$e = C_c^T X \quad (26)$$

where

$$A_c = \begin{pmatrix} 0 & 1 \\ -a_2 & -a_1 \end{pmatrix}; B_c = \begin{pmatrix} 0 \\ b \end{pmatrix}; C_c = \begin{pmatrix} 1 \\ 0 \end{pmatrix};$$

$$X = \begin{pmatrix} e \\ \dot{e} \end{pmatrix}; \tilde{\theta} = \begin{pmatrix} \tilde{k} \\ \tilde{l} \end{pmatrix}; \omega = \begin{pmatrix} y_p \\ r \end{pmatrix}$$

Eq. 25 can be written as

$$\dot{X} = A_c X + \bar{B}_c \rho^* \tilde{\theta}^T \omega; \quad (27)$$

where $\bar{B}_c = B_c l^*$; $\rho^* = 1/l^*$; $e = C_c^T X$. Consider the Lyapunov-like function

$$V(\tilde{\theta}, X) = \frac{X^T P_c X}{2} + \frac{\tilde{\theta}^T \Gamma^{-1} \tilde{\theta}}{2} |\rho^*| \quad (28)$$

where $\Gamma = \Gamma^T > 0$ and $P_c = P_c^T > 0$ and satisfies the algebraic equations

$$P_c A_c + A_c^T P_c = -q q^T - \nu_c L_c \quad (29)$$

$$P_c \bar{B}_c = C_c \quad (30)$$

where q is a vector, $L_c = L_c^T > 0$ and $\nu_c > 0$ is a small constant, that are implied by the Meyer-Kalman-Yakubovich (MKY) lemma (Ioannou and Sun, 1996). The time derivative \dot{V} of V along the solution of Eq. 27 is given by

$$\dot{V} = -\frac{X^T q q^T X}{2} - \frac{\nu_c}{2} X^T L_c X + X^T P_c \bar{B}_c \rho^* \tilde{\theta}^T \omega + \tilde{\theta}^T \Gamma^{-1} \dot{\tilde{\theta}} |\rho^*| \quad (31)$$

Since $X^T P_c \bar{B}_c = X^T C_c = [C_c^T X]^T = e$ and $\rho^* = |\rho^*| \text{sgn}(\rho^*)$, we can make $\dot{V} \leq 0$ by choosing

$$\dot{\tilde{\theta}} = \dot{\theta} = \Gamma e \omega \text{sgn}(\rho^*) \quad (32)$$

Table 1. Performance of MRAC on different road profiles

Profile or Cycle	ITAE error
UDDS	40.5
Federal Test Procedure	42.76
US06	55.13
Highway Fuel Economy Test	11.09
Extra Urban Driving Cycle	8.20
Indian Highway Profile	10.20

which leads to

$$\dot{V} = -\frac{X^T q q^T X}{2} - \frac{\nu_c}{2} X^T L_c X \quad (33)$$

which is negative definite. Hence, using the MRAC adaptation mechanism, we can ensure stability as well as improve the performance by adding the PD controller.

The Environmental Protection Agency (EPA) reviews and revises as necessary the regulations governing the Federal Test Procedures (FTP) to insure that vehicles are tested under circumstances which reflect the actual current driving conditions under which motor vehicles are used, including conditions relating to fuel, temperature, acceleration, and altitude. The adaptive controller was tested on a variety of profiles. The controller was designed for the UDDS profile using the linearized model represented by eq. 7 and the same settings were employed for the remaining profiles. The resulting adaptive controller was implemented on the *nonlinear* model given in Appendix A. The Integrated Time Averaged Error (ITAE) was computed for each power profile. The results are shown in Table 1. It is observed that the adaptive controller with derivative action is able to track power profiles resulting from a wide variety of road conditions. A PID tuning procedure for the UDDS profile resulted in an ITAE error of 91.46. However, this controller when implemented on the US HWY profile resulted in loss of stability. On the other hand, the adaptive controller that was designed for the UDDS profile was able to successfully track the Federal Test Procedure profile, the US06 profile, the Highway Fuel Economy Test profile, the Extra Urban Driving Cycle profile, and the Indian Highway profile with no off-line tuning.

4. CONCLUSIONS

A model reference adaptive controller was designed based on the Lyapunov approach and was shown to perform better than a conventional PID controller for a variety of different power profiles. The adaptability of the controller was tested by implementing the controller on different power profiles which simulate actual power requirement of different road conditions. It was shown that the same controller was successful in tracking a wide

variety of different power profiles without the need for off-line retuning.

ACKNOWLEDGMENTS

Funding from Custom Manufacturing and Engineering, Inc. as well as Florida State University is gratefully acknowledged.

REFERENCES

- [1] Ioannou P. and J. Sun, *Robust Adaptive Control*, Prentice Hall, Inc., 1996
- [2] Kolavennu, P.K., Telotte, J.C., and Palanki, S., "Design of a Fuel Cell Power System for Automotive Applications," *Int. J. Chemical Reactor Engng*, Vol 4: A19 (2006a)
- [3] Kolavennu, P.K., Palanki, S., and Telotte, J.C., ADCHEM 2006, Gramado, Brazil, April 2-5 (2006b)
- [4] Lovins, A.B., and Williams, B.D., "A strategy for the hydrogen transition," *10th Annual U.S. Hydrogen Meeting*, Vienna, Virginia, April 1999
- [5] National Renewable Energy Laboratory, "ADVISOR (Advanced Vehicle Simulator)", 2002
- [6] Pukrushpan, J. T., *Modeling and Control of Fuel Cell Systems and Fuel Processors*, PhD thesis, The University of Michigan, Ann Arbor, 2003
- [7] Zalc, J.M., and Loffler, D.G., "Fuel processing for PEM fuel cells: transport and kinetic issues of system design," *J. Power Sources*, 111, 58-64 (2002)

APPENDIX A

A reduced order model was obtained by suitably substituting the algebraic expressions in the dynamic equations developed by Pukrushpan (2003). The model contains nine states which are defined as m_{O_2} : mass of O_2 in cathode, m_{H_2} : mass of H_2 in anode, m_{N_2} : mass of N_2 in cathode, w_{cp} compressor speed, P_{sm} : supply manifold pressure, m_{sm} : mass inside manifold, P_{rm} : return manifold pressure, $m_{v,an}$: water vapor mass in anode, $m_{v,ca}$: water vapor mass in cathode.

$$\begin{aligned}
\frac{dm_{O_2}}{dt} &= X_{O_2,in} K_{ca,in} \left(P_{sm} - \frac{(m_{O_2}/M_{O_2} + m_{N_2}/M_{N_2} + m_{v,ca}/M_v)RT_{st}}{V_{ca}} \right) \\
&\quad - \left(\frac{m_{O_2}}{m_{O_2} + m_{N_2} + m_{v,ca}} \right) K_{ca,out} \left(\frac{(m_{O_2}/M_{O_2} + m_{N_2}/M_{N_2} + m_{v,ca}/M_v)RT_{st}}{V_{ca}} - P_{rm} \right) \\
&\quad - \frac{M_{O_2} n I_{st}}{4F} \\
\frac{dm_{H_2}}{dt} &= K_1 K_2 P_{sm} - K_1 \frac{(m_{H_2}/M_{H_2} + m_{v,an}/M_v)RT}{V_{gn}} - \frac{M_{H_2} n I_{st}}{2F} \\
\frac{dm_{N_2}}{dt} &= \left(\frac{M_{N_2}}{M_{O_2}} \right) \left(\frac{79}{21} \right) X_{O_2,in} K_{ca,in} \left(P_{sm} - \frac{(m_{O_2}/M_{O_2} + m_{N_2}/M_{N_2} + m_{v,ca}/M_v)RT_{st}}{V_{ca}} \right) \\
&\quad - \left(\frac{m_{N_2}}{m_{O_2} + m_{N_2} + m_{v,ca}} \right) K_{ca,out} \left(\frac{(m_{O_2}/M_{O_2} + m_{N_2}/M_{N_2} + m_{v,ca}/M_v)RT_{st}}{V_{ca}} - P_{rm} \right) \\
\frac{dw_{cp}}{dt} &= \frac{\eta_{cm} k_t}{J_{cp} R_{cm}} (v_{cm} - k_v w_{cp}) - \frac{C_p T_{atm}}{J_{cp} \eta_{cp} w_{cp}} \left(\left(\frac{P_{sm}}{P_{atm}} \right)^{\frac{\gamma-1}{\gamma}} - 1 \right) W_{cp} \\
\frac{dP_{sm}}{dt} &= \left(\frac{\gamma R}{V_{sm}} \right) T_{atm} \left(\frac{P_{sm}}{P_{atm}} \right)^{\frac{\gamma-1}{\gamma}} W_{cp} \\
&\quad - \frac{\gamma P_{sm}}{m_{sm}} K_{ca,in} \left(P_{sm} - \frac{(m_{O_2}/M_{O_2} + m_{N_2}/M_{N_2} + m_{v,ca}/M_v)RT_{st}}{V_{ca}} \right) \\
\frac{dm_{sm}}{dt} &= W_{cp} - K_{ca,in} \left(P_{sm} - \frac{(m_{O_2}/M_{O_2} + m_{N_2}/M_{N_2} + m_{v,ca}/M_v)RT_{st}}{V_{ca}} \right) \\
\frac{dP_{rm}}{dt} &= \frac{RT_{st}}{V_{rm}} \left(K_{ca,out} \left(\frac{(m_{O_2}/M_{O_2} + m_{N_2}/M_{N_2} + m_{v,ca}/M_v)RT_{st}}{V_{ca}} - P_{rm} \right) \right. \\
&\quad \left. - \frac{C_D A_T P_{rm}}{\sqrt{RT_{st}}} \left(\left(\frac{P_{atm}}{P_{rm}} \right)^{\frac{1}{\gamma}} \left(\frac{2\gamma}{\gamma-1} \left(1 - \left(\frac{P_{atm}}{P_{rm}} \right)^{\frac{\gamma-1}{\gamma}} \right)^{\frac{1}{\gamma}} \right) \right) \right) \\
\frac{dm_{v,an}}{dt} &= \left(\frac{M_v}{M_{H_2}} \right) \left(\frac{P_v^{sat}}{\frac{(m_{H_2}/M_{H_2} + m_{v,an}/M_v)RT}{V_{an}} - P_v^{sat}} \right) K_1 \left(K_2 P_{sm} - \frac{(m_{H_2}/M_{H_2} + m_{v,an}/M_v)RT}{V_{an}} \right) \\
&\quad - \frac{M_v A_{fc} n}{F} n_d I_{st} + \frac{D_w}{t_m} (C_{v,ca} - C_{v,an}) \\
\frac{dm_{v,ca}}{dt} &= \left(\frac{\phi_{des} P_{sat}}{P_{sm}} \right) \left(\frac{M_v}{M_a} \right) K_{ca,in} \left(P_{sm} - \frac{(m_{O_2}/M_{O_2} + m_{N_2}/M_{N_2} + m_{v,ca}/M_v)RT_{st}}{V_{ca}} \right) \\
&\quad - \left(\frac{m_{v,an}}{m_{O_2} + m_{N_2} + m_{v,an}} \right) K_{ca,out} \left(\frac{(m_{O_2}/M_{O_2} + m_{N_2}/M_{N_2} + m_{v,ca}/M_v)RT_{st}}{V_{ca}} - P_{rm} \right) \\
&\quad + \left(\frac{M_v n}{2F} \right) I_{st} + \left(\frac{M_v A_{fc} n}{2F} \right) n_d I_{st} \\
&\quad - \frac{D_w}{t_m} (C_{v,ca} - C_{v,an})
\end{aligned} \tag{34}$$